A Silicon Microstrip System equipped with the RX64DTH ASIC for dual energy mammography

L. Ramello, C. Avila, D. Bollini, A.E. Cabal Rodriguez, C. Ceballos Sanchez, W. Dabrowski, A. Diaz Garcia, M. Gambaccini, P. Giubellino, P. Grybos, J. Lopez Gaitan, A. Marzari-Chiesa, L.M. Montano, F. Prino, J.C. Sanabria, A. Sarnelli, K. Swientek, A. Taibi, A. Tuffanelli, P. Van Espen and P. Wiacek

***Abstract*— We present results obtained with a single photon counting system of 384 silicon microstrips (100 micron pitch) equipped with six RX64DTH ASICs including charge preamplifier, shaper, two discriminators and two 20-bit counters for each channel. The energy resolution of the system was determined to be of 0.72 keV (rms) with a spread of threshold setting of 0.32 keV for the whole 384-channel module (at energies of 29-33 keV), indicating its excellent potential for dual-energy imaging. Images of a mammographic test object made of PMMA, polyethylene and water were taken in scanning mode (strips parallel to incoming X-rays) under the dual energy X-ray beams. Images were subsequently processed with the dual energy subtraction technique (Alvarez and Macovski, 1976). Experimental results agree well with MCNP simulations of the mammographic phantom and demonstrate the capability of our system to obtain contrast cancellation between two kinds of materials, thereby enhancing the visibility of small features in the third material.**

***Index Terms*— Silicon detector, microstrip, ASIC, single photon counting, mammography, dual energy.**

I. Introduction

BREAST cancer is a common tumoral affection among female population; as for many cancer types, best results from its treatment are obtained when detection is made in its early stage. Conventional screen-film mammography, which is widely used for initial detection of suspicious cancerous lesions, presents limitations in detecting small lesions on soft tissue, specially in the presence of dense glandular tissue. To overcome this limitation, several efforts have been made to develop digital mammography systems based on solid state detectors. One of the advantages of digital mammography is the image post-processing capability, which increases the possibility of detecting small lesions.

Dual-energy radiography is an effective technique proposed by Alvarez and Macovski [1] and Lehmann *et al* [2], which allows removal of contrast between pairs of tissues by combining two images acquired at different energies. In this way it is possible to improve the contrast of details of interest, by removing the "cluttered" background [3], [4]. While truly monochromatic synchrotron radiation is the best choice for the dual-energy technique, another implementation which uses quasi-monochromatic beams generated with a conventional X-ray tube has recently become available [5], offering an interesting image quality at much reduced cost.

The development of a silicon strip detector and of the associated VLSI electronics with single photon counting capability was carried out in the last few years [6]–[10]. Mammographic imaging experiments were performed in 2002 and 2003 at the quasi-monochromatic beam facility located at University of Ferrara; preliminary results were previously reported [11], [12]. In parallel, angiographic imaging was also investigated at the iodine K-edge energy using the set-up located at University of Bologna [13]–[15].

The aim of the present work is to investigate the imaging capabilities of such a digital single photon counting system, using a three component mammographic phantom. For this purpose the Alvarez-Macovski algorithm was applied to data obtained from the two successive experiments as well as to those obtained from a Monte Carlo simulation of the experimental set-up. For the simulation the particle transport code MCNP-4C was used [16].

II. The Alvarez and Macovski algorithm

The contrast cancellation algorithm was proposed by Alvarez and Macovski [1] and Lehmann *et al* [2]. It is based on the decomposition of mass attenuation coefficient of any material ξ in a linear combination of the coefficients of two basis materials α and β :

$$\frac{\mu_\xi(E)}{\rho_\xi} = a_1 \frac{\mu_\alpha(E)}{\rho_\alpha} + a_2 \frac{\mu_\beta(E)}{\rho_\beta} \qquad (1)$$

Multiplying equation (1) by the thickness and density of the material ξ, the logarithmic transmission can be expressed as a combination of the linear attenuation coefficients of the base

L. Ramello is with Dip. Scienze e Tecnologie Avanzate, Università del Piemonte Orientale and INFN, Alessandria, Italy.

C. Avila, J. Lopez Gaitan and J.C. Sanabria are with Universidad de los Andes, Bogota, Colombia.

D. Bollini is with Dip. di Fisica, Università di Bologna and INFN, Bologna, Italy.

A.E. Cabal Rodriguez, C. Ceballos Sanchez and A. Diaz Garcia are with CEADEN, Havana, Cuba.

W. Dabrowski, P. Grybos, K. Swientek and P. Wiacek are with Faculty of Physics and Applied Computer Science, AGH University of Science and Technology, Cracow, Poland.

M. Gambaccini, A. Sarnelli, A. Taibi and A. Tuffanelli are with Dip. di Fisica, Università di Ferrara and INFN, Ferrara, Italy.

P. Giubellino and F. Prino are with Sez. di Torino, INFN, Torino, Italy.

A. Marzari-Chiesa is with Dip. di Fisica Sperimentale, Università di Torino and INFN, Torino, Italy.

L.M. Montano is with CINVESTAV, Mexico City, Mexico..

P. Van Espen is with Dept. of Chemistry, University of Antwerp, Antwerp, Belgium.

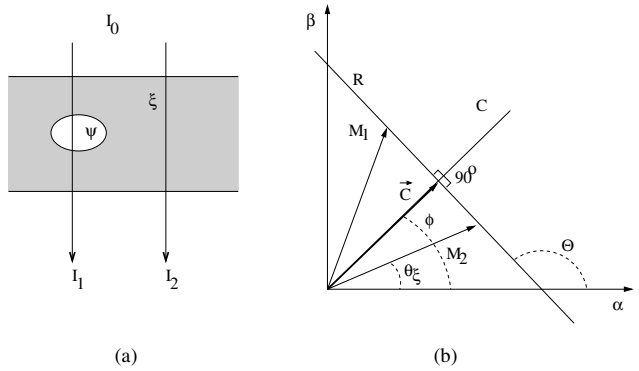

(a) (b)

Fig. 1. (a) A monochromatic X-ray beam I_0 goes through a cavity composed of two different materials (ξ and ψ). (b) Logarithmic transmissions represented in vector form (M_1 and M_2) on a plane formed by the basis materials (α and β). All possible vectors of logarithmic transmission define the line R. C is the projection direction, characterized by the angle ϕ, that is the contrast cancellation angle between ξ and ψ; ϑ_ξ is the characteristic angle of the material ξ.

materials α and β:

$$M = \mu_\xi t_\xi = A_1\mu_\alpha(E) + A_2\mu_\beta(E) \tag{2}$$

For any material ξ, A_1 and A_2 represent the thickness of basis materials that would provide the same X-ray transmission as material ξ.

If the logarithmic transmission M of an absorbing material is measured at two different energies (low and high) E_l and E_h, a system of two equations is obtained [1], [2]. The solution of the system provides the coefficients A_1 and A_2. Aluminum and Lucite have been used in the past as basis materials. For mammography, however, a choice of basis materials with closer attenuation coefficients is required, because of the small differences between the coefficients of normal and tumoral breast tissues. Polymethyl methacrylate (PMMA) and polyethylene (PE) have been chosen as basis materials (α and β) [2].

If a further material ψ is replacing some volume of material ξ (see figure 1(a)), then the contrast between ξ and ψ can be forced to vanish.

Lehmann *et al* [2] have shown the convenience of representing M by a vector in a two dimensional basis plane. In figure 1(a) I_1 is the fraction the beam I_0 transmitted through a thickness of material ξ and a thickness of material ψ, while I_2 is the fraction of I_0 transmitted only through material ξ.

In figure 1(b) the vertex of the vectors M_1 and M_2 (associated respectively to I_1 and I_2) lies on a line R with slope:

$$\Theta = \arctan\left[\frac{\rho_\alpha}{\rho_\beta}\left(\frac{\rho_\xi a_{2\xi} - \rho_\psi a_{2\psi}}{\rho_\xi a_{1\xi} - \rho_\psi a_{1\psi}}\right)\right] \tag{3}$$

which only depends on the characteristics of the two basis materials (α and β) and the two materials ξ and ψ. Associating a gray level to the modulus of each vector we obtain the radiographic images. If a direction C perpendicular to R is considered, the projections of logarithmic transmission vectors M_1 and M_2 along C have the same modulus so that the gray level associated with materials ξ and ψ in the projected image is the same. The direction C is defined in the basis plane by an angle $\phi = \Theta - 90^\circ$ which is called contrast cancellation angle.

An hybrid image $\vec{C}$ is calculated pixel-by-pixel with the projection formula:

$$\vec{C} = A_1\cos\phi + A_2\sin\phi \tag{4}$$

where A_1 and A_2 are given by the solution of the system of two equations like (2). When ϕ is the contrast cancellation angle, the contrast between materials ξ and ψ cancels in the hybrid image, thus enhancing the contrast with some third material. Knowing the attenuation coefficients of the materials at both energies, a theoretical value of ϕ can be computed using equation (3).

III. Experimental setup

The system is intended for imaging with X-rays of relatively low energy (16-40 keV) and has single photon counting capability in order to minimize the dose required to obtain a good quality diagnostic image. The polychromatic beam produced by a W-anode X-ray tube was diffracted via a mosaic crystal monochromator. The mean energy E of the quasi monochromatic beam is given by the Bragg formula

$$E = \frac{nhc}{2d\sin\vartheta_B} \tag{5}$$

where d is the distance between the lattice planes of the highly oriented pyrolitic graphite (HOPG) crystal, n=1,2,3,... is the diffraction order, h is the Planck constant and ϑ_B the Bragg angle [4]. Using the first two diffraction orders a dichromatic beam was produced. Three couples of energies have been used for these measurements: 16-32 keV, 18-36 keV and 20-40 keV. The beam spot was rectangular, with dimensions of 68 mm along the main axis and 8 mm in the perpendicular direction.

Silicon has been chosen as the detector material out of simplicity and reliability considerations; however, due to the low photoelectric absorption probability in the standard thickness of 300 μm, the strips must be oriented parallel to the incoming X-rays [14]. A strip length of 1 cm provides acceptable conversion efficiency at the upper energy of 40 keV. The strip pitch of 100 μm was chosen both because it is a standard in digital mammography and because no significant gain in spatial resolution is expected when going to lower values such as 50 μm [6]; a detailed simulation has shown [17] that in the latter case the number of counts in the low energy tail coming from the high energy component of the beam is about doubled.

The most critical component of the system is the RX64DTH ASIC [10], which provides an energy resolution of 0.8 keV (rms) and the possibility of counting photons in two energy windows, thereby allowing a straightforward use of dual energy imaging techniques. The block diagram of a single electronic channel is shown in Fig. 2. A detector equipped with the RX64 version of the ASIC (with only one discriminator per channel) has been used in the 2002 experiment.

The channel is built of four basic blocks: charge sensitive preamplifier, shaper, two independent discriminators and two independent 20-bit counters. The charge preamplifier integrates

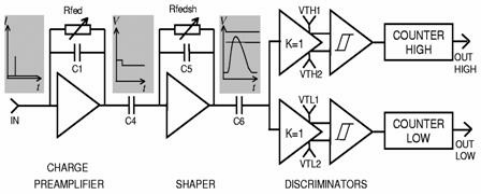

Fig. 2. Block diagram of a single electronic channel of the RX64DTH ASIC.

Fig. 3. The 384-strip detector together with the pitch adapter and 6 RX64DTH ASICs.

the current input signal from a silicon strip detector into a voltage signal. The shaper circuit provides noise filtering and semi-gaussian pulse shaping. Each front-end channel is equipped with two discriminators, which work with separate thresholds. Each readout channel counts pulses which are above the low threshold and independently pulses above the high threshold. Six RX64DTH ASICs have been mounted on a Printed Circuits Board (PCB), together with a 384-strip silicon detector (see Fig. 3). The sensor and the integrated circuits are connected together using a pitch adapter printed on glass and wire bonding. The detector leakage current is typically below 100 pA/strip and the total strip capacitance is about 3 pF.

The system was also tested with six different fluorescence targets (Ge, Zr, Nb, Mo, Ag, Sn) providing six different energies of X-ray radiation. Performing threshold scans of the discriminators of RX64DTH for given energy of X-ray radiation, we have extracted gain, offset and noise in all 384 channels [10]. The measured gain is between 45 and 50 μV/electron and the noise is of about 200 rms electrons, i.e. 0.72 keV (rms) in terms of deposited energy in silicon. We have also determined an effective energy threshold spread in our 384-channel system of 0.32 keV (rms). This means that our system is well adapted for use in dual energy applications.

Data were collected with a program written in LabVIEW 6.0 (National Instruments), while image processing was performed with the Igor Pro 4.05A software [18].

IV. Mammographic images

A test object intended to simulate the three different tissues in the breast, namely adipose, glandular and cancerous, was built with a PMMA base and cylindrical inserts of water and polyethylene, as shown schematically in figure 4.

Profiles of the phantom were taken with three energy settings, namely 16-32, 18-36 and 20-40 keV, which cover the range of energies needed to ensure a good balance between the photon statistics at low and high energy for breasts of different density and thicknesses (see [3], [4]). Images were obtained with two

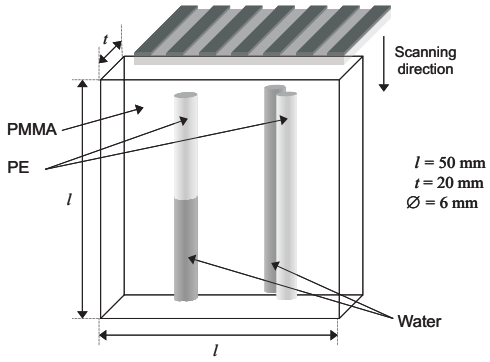

Fig. 4. The mammographic phantom.

similar detectors, one equipped with the RX64 ASIC (in this case two separate exposures at the two energies were necessary) and the second equipped with the RX64DTH ASIC. Due to the translational symmetry of the phantom, scanning along the direction indicated in figure 4 was replaced by two groups of 20 measurements each at two fixed positions in the two halves of the phantom, resulting in a 384×40 pixel matrix; by associating a gray level to the number of counts, the raw images at low and high energy are obtained, as demonstrated in figure 5, referring to the detector equipped with RX64DTH ASICs.

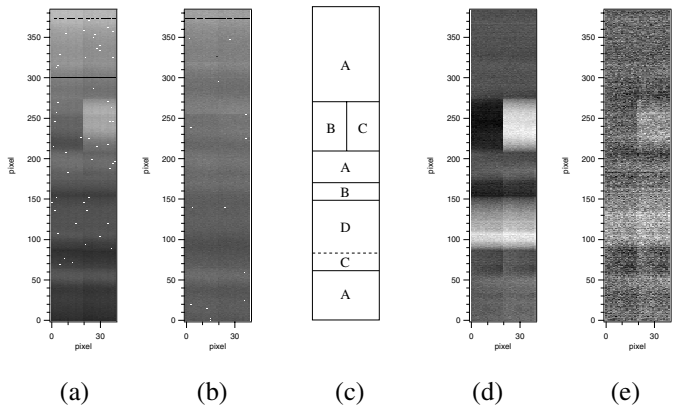

Fig. 5. Panels (a) and (b) show the resulting images of the phantom, obtained for E_l=18 keV and E_h=36 keV respectively, before being corrected; panels (d) and (e) show the same images after being corrected. A scheme (c) of the resolved regions is also shown: (A) PMMA; (B) water; (C) polyethylene; (D) overlap of polyethylene and water. Data taken with RX64DTH ASICs.

The raw images shown in figure 5 (a) and (b) should be corrected before applying the contrast cancellation algorithm. This has been done by means of a fully automatic correction procedure developed using Igor Pro 4.05A [18]. The procedure corrects first for pixel with huge number of counts (appearing as white pixels randomly distributed all over the image), due to errors in the pseudo-random counting conversion procedure. Then a correction for dead channels on the counting ASICs (appearing as black horizontal lines) is applied. A further correction is aimed at fixing the statistical differences among different profiles, appearing in figure 5 (a) and (b) as darker (lighter) vertical lines. These are due to fluctuations in X-

ray intensity or bad synchronization between X-ray exposure and detector readout. The high energy image counts thus corrected are subtracted from the low threshold image. Finally, a correction is applied to account for the spatial distribution of the X-ray beam intensity and other artifacts related to the experimental setup which cause a non-uniform background. This correction is based on 'white-field" profiles (one for each energy) which are measured exposing the detector directly to the X-ray beam. Each phantom profile is divided by the corresponding "white-field" profile normalized to its average value. Figure 5 (d) and (e) shows the images (a) and (b) after being corrected according to the procedure described above.

Figures 6 show the experimental images for each energy pair, again for the detector equipped with the RX64DTH ASICs.

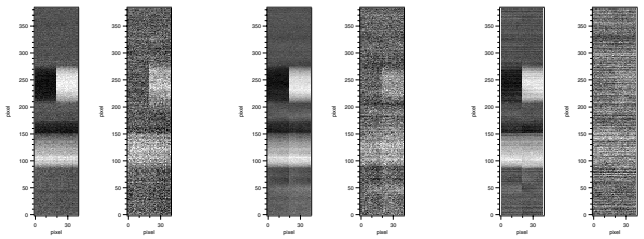

(a) (b) (c) (d) (e) (f)

Fig. 6. Resulting experimental images for E_l=16 keV (a) and E_h=32 keV (b); E_l=18 keV (c) and E_h=36 keV (d); E_l=20 keV (e) and E_h=40 keV (f), obtained with the detector equipped with RX64DTH ASICs.

A simulation of our experiment has been carried out with the MCNP-4C transport code [16]. Incident photons as well as secondary photons and electrons were tracked throughout the phantom and the detector. The simulated profiles in the left and right part of the phantom at the 16-32 keV energy setting are compared in figure 7 to the experimental ones (extracted from figure 6), showing a good agreement.

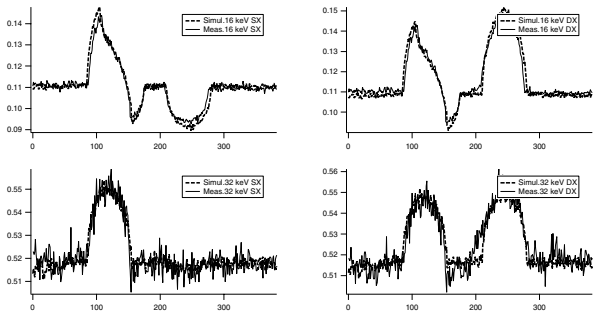

Fig. 7. Superposition of the average measured profiles with the simulated ones at 16 keV (upper plots) and 32 keV (lower plots) for the left and right part of the phantom. Measured profiles taken with the detector equipped with RX64DTH ASICs.

V. RESULTS

In order to obtain the contrast cancellation angle and the projected images for each energy couple, the Alvarez-Macovski

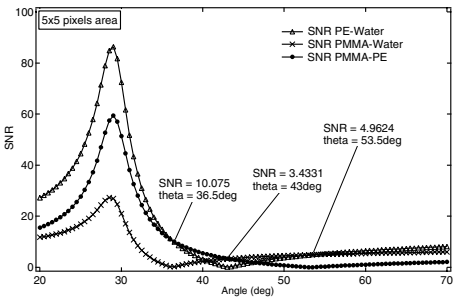

Fig. 8. Experimental result for the Signal-to-Noise Ratio vs. projection angle, for the 16-32 keV energy pair. Data taken with the RX64DTH ASIC.

algorithm was used. To apply the dual energy algorithm, a pixel-by-pixel knowledge of the logarithmic transmission $M = \ln\frac{I_0}{I}$ is required. The intensity I_0 of the incident beam at each energy was calculated from the number of counts I_1 in a region of the phantom where only plexiglass is present. I_0 was then extracted using the theoretical attenuation coefficient of plexiglass at the corresponding energy. Projected images according to equation (4) are then generated for ϕ varying from 20° to 70° in steps of 0.5°.

In order to select the proper contrast cancellation angles, the signal-to-noise ratio (SNR) values for each material couple are calculated. The SNR is defined as the ratio between the signal contrast C_s and the noise contrast C_n. In order to evaluate the SNR on the hybrid images as a function of the projection angle, we assumed that the signal is represented by the relative difference of mean gray level calculated in two regions of the image containing the interesting material pair. For example the signal of water with respect to plexiglass is given by:

$$C_s^{water/plexi} = \frac{m_w - m_p}{m_p} \tag{6}$$

where m_w and m_p are the average of the gray levels measured on a 5×5 pixel homogeneous water and plexiglass area respectively. The contrast of the relative noise has been evaluated on an area A of plexiglass background (35 × 35 pixels). This has been done dividing the area A in 49 sub-images of 5×5 pixels. For each sub-image an average gray level m_i is calculated and then the average m and the standard deviation $\sigma(m)$ of the m_i values are used to define the noise contrast as:

$$C_n = \frac{\sigma(m)}{m} \tag{7}$$

Plotting SNR vs. ϕ at a given energy couple, three curves corresponding to the three material pairs are obtained. Three angles ϕ which minimize the contrast between PE and PMMA, between PE and water and between PMMA and water respectively are found, representing the contrast cancellation angles for each pair of materials.

Figure 8 shows the preliminary SNR vs. ϕ for measured data with RX64DTH at E_l=16 keV and E_h=32 keV: the contrast cancellation angle for each material pair corresponds to the minimum of each curve. Figure 9 shows the SNR vs. ϕ for simulated data at the same energy setting. For all energy

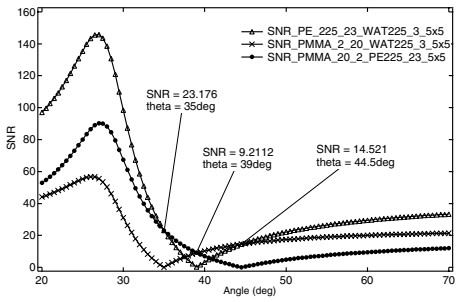

Fig. 9. Simulation result for the Signal-to-Noise Ratio vs. projection angle, for the 16-32 keV energy pair.

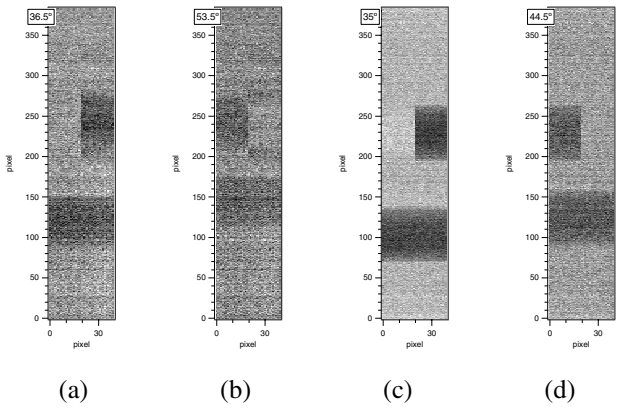

(a) (b) (c) (d)

Fig. 10. Projected images corresponding to the contrast cancellation angle between PMMA and water (a) and between PMMA and PE (b), for experimental images at E_l=16 keV and E_h=32 keV; the same result for simulated images is shown in panels (c) and (d). Data taken with RX64DTH ASICs.

settings, there is a good agreement (within 1.5°) between theoretical, simulated and experimental values of the contrast cancellation angle ϕ for each material pair. The slight mismatch between theory and experiment at some energies could well be due to the presence of a small gradient of counts along the vertical axis of the PMMA areas of the measured images.

Table I summarizes the SNR values measured for both detectors (values for RX64DTH are preliminary) on areas of 5×5 pixels at the measured cancellation angles. The better performance of the RX64DTH ASIC makes it possible to obtain comparable values of SNR with respect to the RX64 with about half of the incident photons. The experimental SNR values are limited mainly by the poor statistics of high energy images (32, 36 and 40 keV) due both to lower number of incident photons and lower detector efficiency.

TABLE I

VALUES OF SNR ON A 5×5 PIXEL AREA AT THE MEASURED CONTRAST CANCELLATION ANGLES, FOR BOTH DETECTORS.

Energy (keV)	**Canceled materials**	**Contrast material**	**SNR**	
			RX64	**RX64DTH**
16-32	PMMA-Water	PE	4.35	10.1
	PE-Water	PMMA	1.60	3.4
	PE-PMMA	Water	2.70	5.0
18-36	PMMA-Water	PE	8.86	6.1
	PE-Water	PMMA	1.92	2.2
	PE-PMMA	Water	2.30	3.4
20-40	PMMA-Water	PE	2.55	2.2
	PE-Water	PMMA	0.67	0.8
	PE-PMMA	Water	0.89	1.0

Figure 10 shows the hybrid images obtained projecting the experimental and simulated images at E_l=16 keV and E_h=32 keV using the contrast cancellation angles determined as explained above. Panels (a) and (c) show the image at the cancellation angle between PMMA and water, where only the PE can be seen. Similarly, panels (b) and (d) show the image at the cancellation angle between PMMA and PE, where only the water can be seen.

VI. CONCLUSION

We have presented a single photon counting detector equipped with the RX64DTH ASIC, providing digital readout within two selectable energy windows for low energy X-rays. The systems' energy resolution is well adapted to imaging techniques like dual energy mammography and angiography. Imaging tests made with a mammographic phantom consisting of three materials using the Alvarez-Macovski algorithm show contrast cancellation between two materials, thereby enhancing the visibility of small features in the third one.

ACKNOWLEDGMENT

We are grateful to B. Pini and F. Dumitrache for help with assembly of detectors and ASICs, to E. Filoni for the layout of the pitch adapter and to F. Rotondo for help with cabling. R. Wheadon gave us precious assistance in setting up the automated bonding procedure. This work was supported by the European Union ALFA Programme (Contract N. AML/B7-311/97/0666/II-0042) and by the Polish State Committee for Scientific Research (Grant N. 3T11B01427).

REFERENCES

[1] R. E. Alvarez and A. Macovski, *Phys. Med. Biol.*, **21**, 733-744 (1976).
[2] L. A. Lehmann et al., *Med. Phys.*, **8**, 659-667 (1981).
[3] S. Fabbri et al., *Phys. Med. Biol.*, **47**, 1-13 (2002).
[4] M. Marziani et al., *Phys. Med. Biol.*, **47**, 305-313 (2002).
[5] M. Gambaccini et al., *Nucl. Instr. and Meth.*, **A365**, 248-254 (1995).
[6] W. Dabrowski et al., *Nucl. Instr. and Meth.*, **A442**, 346-354 (2000).
[7] P. Grybos and W. Dabrowski, *IEEE Trans. Nucl. Sci.*, **48**, 466-472 (2001).
[8] P. Grybos et al., *Microelectronics Reliability*, **42**, 427 (2002).
[9] D. Bollini et al., *Nucl. Instr. and Meth.*, **A515**, 458-466 (2003).
[10] P. Grybos et al., "RX64DTH - A fully integrated 64-channel ASIC for digital X-ray imaging system with energy window selection" *IEEE NSS-MIC Conference*, this Conference Record (2004).
[11] G. Baldazzi et al., *AIP Conf. Proc.*, Vol. **682**, 14-23 (2003).
[12] A.E. Cabal Rodriguez et al., "X-ray imaging with a single photon counting system" *Proc. EXRS 2004 Eur. Conf. on X-Ray Spectrometry*, Alghero, Italy (2004).
[13] G. Baldazzi et al., *Nucl. Instr. and Meth.*, **A509**, 315-320 (2003).
[14] G. Baldazzi et al., *Nucl. Instr. and Meth.*, **A514**, 206-214 (2003).
[15] A. Sarnelli et al., *Phys. Med. Biol.*, **49**, 3291-3305 (2004).
[16] "MCNP 4C-Monte Carlo N-Particle Transport Code System." *RSICC Computer Code Collection, Oak Ridge National Laboratory* (2001).
[17] G. Baldazzi et al., *Nucl. Instr. and Meth.*, **B213**, 603-606 (2004).
[18] "IgorPro 4.05A Manual" *WaveMetrics Inc., Lake Oswego* (2002).